Journal of Sound and Vibration (2002) **249**(1), 3–22
doi:10.1006/jsvi.2001.3645, available online at http://www.idealibrary.com on IDEAL®

POWER FLOW ANALYSIS OF INDETERMINATE ROD/BEAM SYSTEMS USING A SUBSTRUCTURE METHOD

Z. H. Wang, J. T. Xing and W. G. Price

School of Engineering Sciences, Ship Science, University of Southampton, Southampton SO17 1BJ, England

(*Received* 5 *May* 2000, *and in final form* 6 *February* 2001)

Based on the concepts of a subsystem structural dynamics approach, a general power flow analysis of an indeterminate vibrating system consisting of three rods is presented and discussed. This is achieved by complementing the normal dynamic equations with geometrical compatibility equations allowing assessment of power flow dynamic characteristics applied to and excited within the system. The method may be classified as a form of substructuring using free–free interface conditions. The displacement contribution of the external and boundary coupling forces is deduced, permitting the power flow between the interfaces of substructures to be determined. The method presented is used in a power flow analysis of a simple rod truss system and in a more complex system as demonstrated.

1. INTRODUCTION

Many types of engineering structures are subjected to high-frequency excitation, in the sense that high modal densities are experienced in the high-frequency range. A power flow analysis (PFA) provides a technique able to model the high-frequency dynamic responses of structural dynamical systems of high modal density. PFA and Statistical Energy Analysis (SEA) [1–5] techniques demonstrate similarities of approach involving the division of a structure into substructures and a time-averaged vibrational energy or power parameter used to describe the response of a substructure.

The theoretical basis of SEA has developed because of the deficiencies of finite element and other methods to analyze accurately the structural dynamic response of a system excited at high frequencies. Fahy [1] presents a comprehensive critical review of SEA theory highlighting its origin, development and future possible direction and applications. One of the earliest applications of SEA to describe and analyze simple vibrating systems was presented by Lyon and Maidanik [2], who formulated a mathematical method based on modal theory. Lyon [3] further developed their ideas with applications to more complex vibrating systems. Langley [4] described a wave theory approach and a mobility model was proposed by Manning [5]. Keane and Price [6] and Fahy and Price [7] present recent developments and advances in SEA theory and its mathematical modelling with applications to complex, coupled vibrating systems.

The PFA approach is not necessarily restricted to the high-frequency range and the parameters of power flow and mobility may be expressed as a modal function aggregation to retain the resonant behaviours of the individual and global structures at low modal density. The mobilities describing finite substructures may be expressed in an equivalent

0022-460X/02/010003 + 20 $35.00/0

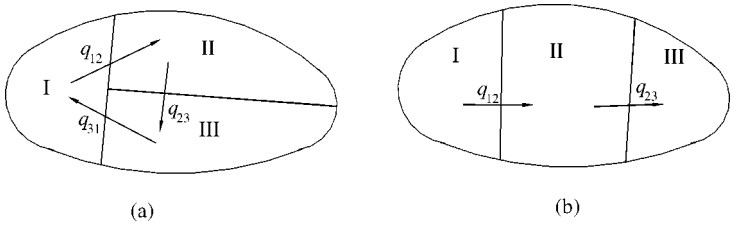

Figure 1. Schematic illustration of a system with three subsystems I–III. The arrows indicate energy flow from one subsystem to another. In the indeterminate system of (a), a delta energy flow pattern occurs and three energy flow quantities are required to analyze the energy flow in the system. In contrast, the sequential energy flow pattern observed in (b) requires only two energy flows to analyze the system.

manner to infinite substructures at high modal density and therefore the results are similar to those obtained by SEA [3].

One of the earliest concepts of PFA to describe and analyze simple vibrating systems was presented by Lyon and Maidanik [2]. Goyder and White [8–10] used the rate of energy flow to characterize the dynamic response of the vibrating system and described the power flow through the isolation system. This was found to be a more meaningful parameter in assessing the dynamic properties of isolator–engine systems as confirmed by Pinnington and White [11]. Xing and Price [12, 13] developed the concept of an energy flow density vector which uniquely defines the energy transmission between one part of a system and another in the continuum system.

To study the energy flow in a vibrating system or continuum adopting either a statistical energy analysis or a power flow analysis it is necessary to divide the continuum domain or system into a number of subsystems. For illustrative purposes, Figure 1 schematically shows a continuum divided into three subdomains (I, II, III), but with different configurations. For Figure 1(a), Xing and Price [13] showed that three energy flows q_{ij}, forming a *delta flow pattern*, are required in a PFA approach, whereas only two energy flows, forming a *sequential flow pattern*, are required to analyze the subsystem configuration in Figure 1(b). They also demonstrated that because the number of independent energy flow equations for three subdomains is two, the delta flow pattern cannot be determined solely from an energy flow balance analysis. In fact, the energy flow lines in Figure 1(a) form a closed curve, i.e., a conceptual delta shape, so that any quantity of energy flow added will not affect the energy flow balance, further confirming that the subdivided system of Figure 1(a) cannot be determined only by examination of the equation of energy flow balance.

For frame structures, several PFA approaches have been presented which combine the exact solution of individual structural elements. These include the mobility approach in L-shaped plates by Cuschieri [14], the direct dynamic stiffness method in a general frame by Langley [15] and a travelling wave and scattering approach to a beam frame by Miller and Flotow [16], Horner and White [17], Beale and Accorsi [18]. The beam frame systems described in references [16–18] are indeterminate vibrating systems and displacement boundary conditions in the coupling edges are applied to solve these problems. For indeterminate vibrating systems, the main differences exhibited in the PFA approaches lie in the different methods used to calculate the response of subsystems. For example, in references [16–18], a travelling wave method is developed whereas Shankar and Keane [19, 20] employ finite element methods.

This paper examines an indeterminate vibrating system consisting of three rods. It is a segment of a rod–truss system, which is used widely in engineering. Usually, only

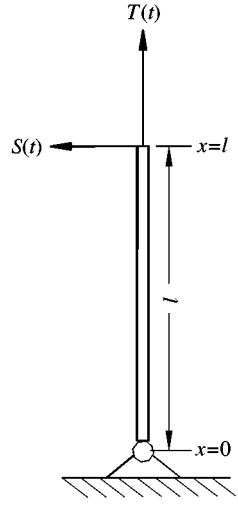

Figure 2. A single uniform rod system.

compressive responses in the rod are considered in a static analysis and/or in a low modal density range analysis of the rod–truss system, but herein bending influence is also examined because there may be many bending modes in the frequency range under investigation. A theoretical modal substructure approach is used to evaluate the vibration power flow characteristics of the posed simple three-rod system. Hence, natural frequencies and mode shapes of the single rod are first determined and then a mobility function or frequency response function is derived for the coupled three-rod system. This is achieved by introducing geometrical compatibility conditions which supplement the normal dynamic equations describing the vibrating characteristic of the indeterminate system. Both instantaneous and time-averaged power flows in the rod system are calculated and their characteristics discussed. The modal substructure approach presented can readily take into account variations in substructure damping and can also be applied to a more complex structure as is further demonstrated.

2. MOBILITY FUNCTION AND POWER FLOW OF A SUBSYSTEM

Figure 2 illustrates a simple subsystem of the rod system shown later. Here it is treated as an idealized system consisting of a single uniform rod of length l hinged at its base $x = 0$ with a free end at $x = l$. This rod of uniform cross-section area A and moment of inertia I is made of material of mass density ρ, elastic Young's modulus E and its structural damping properties are represented by a linear Voigt viscoelastic model with hysteretic damping or loss factor η. The harmonic axial and transverse exciting forces per unit length applied to the free end are

$$T(t) = T_0 e^{i\omega t} \quad \text{and} \quad S(t) = S_0 e^{i\omega t}, \tag{1}$$

respectively, where i denotes the square root of -1 and ω the frequency of excitation.

It is assumed that the axial and transverse responses of the rod are uncoupled. The equation of motion describing the axial displacement $u(x, t)$ (see, for example, reference

[21]) is given in the form

$$-EA(1+\mathrm{i}\eta)\frac{\partial^2 u(x,t)}{\partial x^2}+\rho A\frac{\partial^2 u(x,t)}{\partial t^2}=T(t)\,\delta(l-x), \tag{2}$$

where $\delta(x)$ denotes the *Dirac* delta function.

According to a theorem by Rayleigh [22], any distortion of the rod may be expressed as an aggregate of distortions in its principal modes. That is

$$u(x,t)=\sum_{r=1}^{n} u_r(x)\,p_r(t), \tag{3}$$

where $u_r(x)$ is the rth principal mode shape, $p_r(t)$ denotes the rth principal co-ordinate and n modes are admitted into the analysis. For the axial vibration of the simple system under examination

$$u_r(x)=\sin k_r x=\sin\left(\frac{(2r-1)}{2l}\,\pi x\right) \tag{4}$$

and the rth natural frequency is given by

$$\omega_r=k_r\sqrt{\frac{E}{\rho}}=\left(\frac{(2r-1)}{2l}\,\pi\right)\sqrt{\frac{E}{\rho}}\,. \tag{5}$$

When the assumed solution is substituted into the equation of motion and the resulting equation is multiplied by $u_s(x)$ prior to integrating with respect to x over the length of the rod, the equation describing the rth principal co-ordinate $p_r(t)$ is expressed as

$$A[E(1+\mathrm{i}\eta)\,k_r^2 p_r(t)+\rho\ddot{p}_r(t)]\int_0^l \sin^2(k_r x)\,\mathrm{d}x=\int_0^l \sin(k_r x)\,T(t)\,\delta(l-x)\,\mathrm{d}x \tag{6}$$

for $r=1, 2, 3, \ldots, n$. After using equations (1) and (4), the principal co-ordinate is defined by the expression

$$\begin{aligned} p_r(t)&=\frac{2(-1)^{r+1}T_0}{[-\rho\omega^2+E(1+\mathrm{i}\eta)k_r^2]Al}\,\mathrm{e}^{\mathrm{i}\omega t}\\ &=\frac{2[(\omega_r^2-\omega^2)-\mathrm{i}\eta\omega_r^2]\sin(k_r l)T_0}{m[(\omega_r^2-\omega^2)^2+\eta^2\omega_r^4]}\,\mathrm{e}^{\mathrm{i}\omega t}, \end{aligned} \tag{7}$$

where $m=\rho Al$ is the mass of the rod. The substitution of equations (4) and (7) into equation (3) gives the axial displacement of the rod at position x, $0\leqslant x\leqslant l$. That is

$$u(x,t)=\frac{2}{m}\sum_{r=1}^{n}\frac{[(\omega_r^2-\omega^2)-\mathrm{i}\eta\omega_r^2](-1)^{r+1}\sin(k_r x)F(l)}{[(\omega_r^2-\omega^2)^2+\eta^2\omega_r^4]}\,\mathrm{e}^{\mathrm{i}\omega t}, \tag{8}$$

together with the vibration velocity,

$$\begin{aligned} \dot{u}(x,t)&=\frac{2}{m}\sum_{r=1}^{n}\frac{\mathrm{i}\omega[(\omega_r^2-\omega^2)-\mathrm{i}\eta\omega_r^2](-1)^{r+1}\sin(k_r x)T_0}{[(\omega_r^2-\omega^2)^2+\eta^2\omega_\gamma^4]}\,\mathrm{e}^{\mathrm{i}\omega t}\\ &=\frac{2}{m}\sum_{r=1}^{n}\frac{\omega|\sin(k_r x)|T_0}{[(\omega_\gamma^2-\omega^2)^2+\eta^2\omega_r^4]^{1/2}}\,\mathrm{e}^{\mathrm{i}(\omega t+\varphi_u)}, \end{aligned} \tag{9}$$

where

$$\varphi_u(x) = \tan^{-1}\left[\sum_{r=1}^{n} \frac{(-1)^{r+1}(\omega_r^2 - \omega^2)\sin(k_r x)}{((\omega_r^2 - \omega^2)^2 + \eta^2\omega_r^4)} \Big/ \sum_{r=1}^{n} \frac{(-1)^{r+1}\eta\omega_r^2 \sin(k_r x)}{((\omega_r^2 - \omega^2)^2 + \eta^2\omega_r^4)}\right]$$

is the phase angle between the velocity and axial exciting force.

Similar to this axial response analysis, the equation of motion describing the transverse bending displacement $w(x, t)$ is given in the form

$$-EI(1 + \mathrm{i}\eta)\frac{\partial^4 w(x, t)}{\partial x^4} + \rho A \frac{\partial^2 w(x, t)}{\partial t^2} = S(t)\,\delta(l - x), \tag{10}$$

where $S(t)$ denotes the transverse exciting force at the end of the rod.

For the system under examination, the natural frequencies and mode shapes (see, for example, reference [23]) are given by

$$\omega_r = \frac{k_r^2}{l^2}\sqrt{\frac{EI}{A\rho}}, \tag{11}$$

$$w_r(x) = \begin{cases} \dfrac{x}{l}, & r = 0 \\ \sin\left(\dfrac{k_r x}{l}\right) + \dfrac{\sin k_r}{\sinh k_r}\sinh\left(\dfrac{k_r x}{l}\right), & r = 1, 2, 3, \ldots, n \end{cases} \tag{12}$$

and

$$k_r \approx \begin{cases} 0 & \text{for } r = 0 \\ 3{\cdot}9266, 7{\cdot}0686, \ldots, (n + 0{\cdot}25)\pi & \text{for } r = 1, 2, \ldots, n. \end{cases} \tag{13}$$

Similar to equation (7), the principal co-ordinate of bending vibration is defined by the expression

$$p_r(t) = \frac{[(\omega_r^2 - \omega^2) - \mathrm{i}\eta\omega_r^2]\, w_r(l) S_0}{[(\omega_r^2 - \omega^2)^2 + \eta^2\omega_r^4]\int_0^l \rho A w_r^2(x)\,\mathrm{d}x}\,\mathrm{e}^{\mathrm{i}\omega t}. \tag{14}$$

Using Rayleigh's theory (equation (3)), the transverse displacement of the rod at position x, $(0 \leqslant x \leqslant l)$ is given by

$$w(x, t) = \sum_{r=0}^{n} \frac{[(\omega_r^2 - \omega^2) - \mathrm{i}\eta\omega_r^2]\, w_r(x) w_r(l)\, S_0}{[(\omega_r^2 - \omega^2)^2 + \eta^2\omega_r^4]\int_0^l \rho A w_r^2(x)\,\mathrm{d}x}\,\mathrm{e}^{\mathrm{i}\omega t}, \tag{15}$$

together with the vibration velocity,

$$\begin{aligned} \dot{w}(x, t) &= \sum_{r=0}^{n} \frac{[\omega\omega_r^2 + \mathrm{i}\omega(\omega_r^2 - \omega^2)] w_r(x) w_r(l) S_0}{[(\omega_r^2 - \omega^2)^2 + \eta^2\omega_r^4]\int_0^l \rho A w_r^2(x)\,\mathrm{d}x}\,\mathrm{e}^{\mathrm{i}\omega t} \\ &= \sum_{r=0}^{n} \frac{\omega w_r(x) w_r(l)\, S_0}{[(\omega_r^2 - \omega^2)^2 + \eta^2\omega_r^4]^{1/2}\int_0^l \rho A w_r^2(x)\,\mathrm{d}x}\,\mathrm{e}^{\mathrm{i}(\omega t + \varphi_w)}, \end{aligned} \tag{16}$$

where

$$\varphi_w(x) = \tan^{-1}\left[\sum_{r=0}^{n} \frac{(\omega_r^2 - \omega^2) w_r(x)\, w_r(l)\, S_0}{[(\omega_\gamma^2 - \omega^2)^2 + \eta^2\omega_r^4]\int_0^l \rho A w_r^2(x)\,\mathrm{d}x} \Big/ \sum_{r=0}^{n} \frac{\eta\omega_r^2 w_r(x) w_r(l)}{[(\omega_\gamma^2 - \omega^2)^2 + \eta^2\omega_r^4]\int_0^l \rho A w_r^2(x)\,\mathrm{d}x}\right]$$

describes the phase angle between the transverse velocity and transverse exciting force.

Assuming that the rod is treated as a simple Euler–Bernoulli beam, it follows that slope $\theta(x, t) = \partial w/\partial x$ and bending moment $M(x, t) = EI\,\partial^2 w/\partial x^2$. A more sophisticated theory may be adopted; e.g., Timoshenko beam, Vlasov beam, etc., which add complications to the analysis without contributing additional insights into the power flow mechanisms.

After accounting for the different ways in which power flows through the rod, the instantaneous power flow in the rod at section x is given by

$$q(x, t) = \mathrm{Re}\{\dot{u}(x, t)\}\,\mathrm{Re}\{T(x, t)\} + \mathrm{Re}\{\dot{w}(x, t)\}\,\mathrm{Re}\{S(x, t)\} + \mathrm{Re}\{\dot{\theta}(x, t)\}\,\mathrm{Re}\{M(x, t)\}, \quad (17)$$

where $T(x,t)$, $S(x,t)$, $M(x,t)$ denote the axial force, transverse shear force and bending moment respectively.

The time-averaged value of power flow over a period of excitation T at position x is given by

$$\langle q(x, t)\rangle = \frac{1}{T}\int_0^T q(x, t)\,\mathrm{d}t. \quad (18)$$

It is easy to obtain all the parameters in equation (17) with $\dot{u}(x, t)$ and $\dot{w}(x, t)$ determined from basic beam theory and given in equations (9, 16) respectively. The definition of power flow given by Goyder and White [8] or Cremer *et al.* [24, chapter 4, equation (129)], i.e., $P = \frac{1}{2}\,\mathrm{Re}\{f(x, t)v^*(x, t)\}$, where $v^*(x, t)$ is the conjugate of the velocity, is the time-averaged power flow of equation (17), and hence, is equivalent to equation (18).

For illustrative purposes and to simplify the analysis, a steel rod of mass $m = 3120$ kg, with properties $\eta = 0{\cdot}015$, $E/\rho = 2{\cdot}69 \times 10^7\ \mathrm{m^2/s^2}$, length $l = 10$ m, section area $A = 0{\cdot}04\ \mathrm{m^2}$ is examined under a unit amplitude excitation in the axial direction. That is, transverse bending is not considered in this example such that the instantaneous power flow in the rod simplifies to

$$\begin{aligned} q(x, t) &= \mathrm{Re}\{\dot{u}(x, t)\}\,\mathrm{Re}\{T(x, t)\} = \mathrm{Re}\{\dot{u}(x)\,\mathrm{e}^{\mathrm{i}(\omega t + \varphi_u(x))}\}\,\mathrm{Re}\{T(x)\mathrm{e}^{\mathrm{i}(\omega t + \varphi_T(x))}\} \\ &= \tfrac{1}{2}\,\dot{u}(x)T(x)[\cos(\varphi_u(x) - \varphi_T(x)) + \cos(2\omega t + \varphi_u(x) + \varphi_T(x))] \\ &= \dot{u}(x)T(x)\cos(\varphi_u(x) - \varphi_T(x))\cos^2(\omega t + \varphi_T(x)) \\ &\quad - \tfrac{1}{2}\,\dot{u}(x)T(x)\sin(\varphi_u(x) - \varphi_T(x))\sin 2(\omega t + \varphi_T(x)), \end{aligned} \quad (19)$$

where $\dot{u}(x)$ and $T(x)$ are the amplitude distributions of axial velocity and traction force, respectively, $\varphi_T(x)$ is the phase angle between the traction force and axial exciting force, $\varphi_u(x)$ is already defined in equation (9). Fahy [25] derived an equivalent equation for the instantaneous sound intensity component. The first term, with a non-zero time-averaged value, represents an active component, corresponding to the local transmission of the energy, that is, the damping dissipation of energy. The second term, with a zero time-averaged value, represents a reactive component, corresponding to the local oscillatory transmission of energy, that is, the local energy exchange between kinetic energy, potential energy and the input energy of excitation.

Figure 3 illustrates the magnitudes of response velocity, traction force and power flow distributed along the rod at frequencies of 200 and 328·9 Hz. The frequency 328·9 Hz corresponds to the resonance frequency of the second natural mode of the rod. The magnitudes of input power and time-averaged input power created by the unit force amplitude excitation are of value $8{\cdot}74 \times 10^{-6}$ W. They are the *same* value because the excitation force and velocity response at the exciting position have the same phase angles and, therefore, the reactive input power is always equal to zero. At the frequency of 200 Hz,

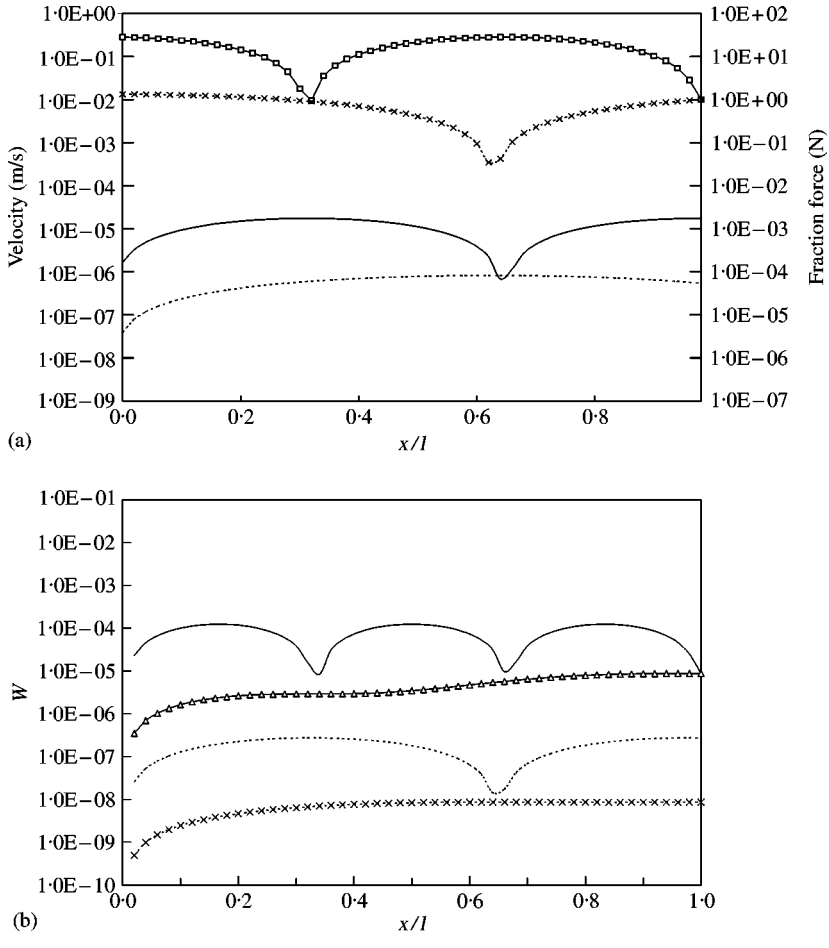

Figure 3. Distribution of the magnitudes of (a) velocity and traction force: ——, velocity at resonance; ----, velocity at non-resonance; —□—, traction force at resonance; --×--, traction force at non-resonance; (b) power flow along the rod at a resonance frequency of 328·9 Hz and a non-resonance frequency of 200 Hz: ——, power flow magnitude (resonance); ----, power flow magnitude (non-resonance); —△—, time-averaged power flow (resonance); --×--, time-averaged power flow (non-resonance).

corresponding to a non-resonance condition, the reactive input power is *not* equal to zero with respective magnitudes of input power and time-averaged input power of values $2{\cdot}71 \times 10^{-7}$ W and $8{\cdot}59 \times 10^{-9}$ W.

As shown in Figure 3(a), at the resonance frequency of 328·9 Hz, the response velocity and traction force along the rod experience minimum values at different positions, thus creating two troughs in the power flow distribution curve as shown in Figure 3(b). At a non-resonance frequency of 200 Hz, only the traction force exhibits a minimum value producing only a single power flow trough at exactly the same position on the rod. The magnitude of instantaneous power flow at any point along the rod (i.e., $0 < x < l$) may be larger than the magnitude of instantaneous input power of the exciting force at $x = l$ due to the influence of resonance. This is because the distribution of phase associated with the reactive power component along the rod in equation (19) varies with position causing the phase at some positions to be opposite in sign to the value at other positions. This implies that some parts of the rod store energy whereas other parts release energy and the rate of

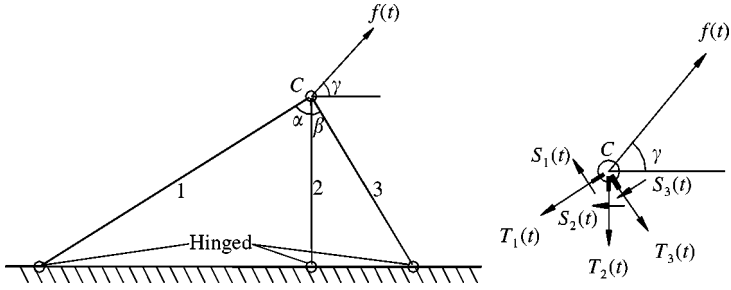

Figure 4. A three-rod indeterminate system.

energy transfer at different sections of the rod may be larger than the input power, but the aggregation of instantaneous power flow along all sections of the rod is equal to the instantaneous input power of the exciting force at any instant time. The distribution curve of the time-averaged power flow does not exhibit troughs along the rod in both resonant and non-resonant conditions as shown in Figure 3(b). The time-averaged power flow values always increase with increasing x along the rod. This is due to the fact that in any period, the time-averaged power flow value in any section x is equal to the rate of total energy dissipation of the rod from sections 0 to x.

3. POWER FLOW IN AN INDETERMINATE THREE-ROD SYSTEM

3.1. BOUNDARY CONDITION AT A JUNCTION

Figure 4 illustrates the three-rod system under examination. It is assumed that each uniform rod is constructed of the same material (i.e., same Young's modulus E and structural damping loss factor η) but of different lengths l_j ($j = 1, 2, 3$), moment of the inertias I_j, cross-sectional areas A_j and masses $m_j = \rho l_j A_j$. For simplicity, rod 2 is assumed to be vertical though this restriction may be removed but this increases algebraic manipulation without producing additional conceptual insights into this study. Each rod is hinged at its base (see also Figure 2) and connected at their ends at C where an external exciting force $f(t) = F e^{i\omega t}$ acts causing axial traction forces $T_j(t)$ and transverse shear forces $S_j(t)$ at C.

Following the discussion of the previous section and because of structural damping, the axial traction force and transverse shear force in each rod at C is expressed in the complex valued form

$$T_j(t) = T_j e^{i(\omega t + \varphi_{T_j})} \qquad S_j(t) = S_j e^{i(\omega t + \varphi_{S_j})}, \tag{20}$$

where φ_{T_j}, φ_{S_j} denote the phase angles between the external force $f(t)$ and axial traction force $T_j(t)$, and the external force $f(t)$ and transverse shear force $S_j(t)$ of the rod j respectively.

For the simplified indeterminate system under examination, the force balance equation at C is given by

$$\begin{aligned} T_1(t)\sin\alpha + S_1(t)\cos\alpha + S_2(t) - T_3(t)\sin\beta + S_3(t)\cos\beta &= f(t)\cos\gamma, \\ T_1(t)\cos\alpha - S_1(t)\sin\alpha + T_2(t) + T_3(t)\cos\beta + S_3(t)\sin\beta &= f(t)\sin\gamma, \end{aligned} \tag{21}$$

where the angles are defined in Figure 4. For solution, this set of equations must be supplemented by a geometrical compatibility equation. That is, the distortions or velocities at point C of the three rods are the same in all directions, thus providing the conditions

$$\begin{aligned}
&\dot{u}_1(t)\sin\alpha + \dot{w}_1(t)\cos\alpha - \dot{w}_2(t) = 0,\\
&\dot{u}_1(t)\cos\alpha - \dot{w}_1(t)\sin\alpha - \dot{w}_2(t) = 0,\\
&-\dot{u}_3(t)\sin\beta + \dot{w}_3(t)\cos\beta - \dot{u}_2(t) = 0,\\
&\dot{u}_3(t)\cos\beta + \dot{w}_3(t)\sin\beta - \dot{u}_2(t) = 0,
\end{aligned} \tag{22}$$

where $\dot{u}_j(t)$, $\dot{w}_j(t)$ denote the axial and transverse velocities, respectively, at point C of the rod j.

It follows from equations (9) and (16) that the axial and transverse velocities at C in each rod of this indeterminate system can be expressed in the form

$$\begin{aligned}
\dot{u}_j(t) &= \frac{2}{m_j}\sum_{r=1}^{n}\frac{\omega T_j(t)}{[(\omega_{r,u_j}^2-\omega^2)^2+\eta^2\omega_{r,u_j}^4]^{1/2}}\,\mathrm{e}^{\mathrm{i}\varphi_{u_j}}\\
&= T_j(t)\,U_j\,\mathrm{e}^{\mathrm{i}\varphi_{u_j}},
\end{aligned} \tag{23}$$

$$\begin{aligned}
\dot{w}_j(t) &= \sum_{r=0}^{n}\frac{\omega w_{r,j}(x)w_{r,j}(l)S_j(t)}{[(\omega_{r,w_j}^2-\omega^2)^2+\eta^2\omega_{r,w_j}^4]^{1/2}\int_0^l \rho A w_{r,j}^2(x)\,\mathrm{d}x}\,\mathrm{e}^{\mathrm{i}\varphi_{w_j}}\\
&= S_j(t)\,W_j\,\mathrm{e}^{\mathrm{i}\varphi_{w_j}},
\end{aligned} \tag{24}$$

where ω_{r,u_j} is the rth natural frequency of axial vibration of the jth rod and φ_{u_j} is the phase angle between axial velocity $\dot{u}_j(t)$ and traction force $T_j(t)$; ω_{r,w_j}, $w_{r,j}$ are the rth natural frequency and mode shape of transverse bending vibration of the jth rod and φ_{w_j} is the phase angle between transverse velocity $\dot{w}_j(t)$ and shear force $S_j(t)$.

From equations (22)–(24), the geometrically compatible equations become

$$\begin{aligned}
&T_1(t)U_1\mathrm{e}^{\mathrm{i}\varphi_{u_1}}\sin\alpha + S_1(t)\,W_1\,\mathrm{e}^{\mathrm{i}\varphi_{w_1}}\cos\alpha - S_2(t)\,W_2\,\mathrm{e}^{\mathrm{i}\varphi_{w_2}} = 0,\\
&T_1(t)U_1\mathrm{e}^{\mathrm{i}\varphi_{u_1}}\cos\alpha - S_1(t)\,W_1\,\mathrm{e}^{\mathrm{i}\varphi_{w_1}}\sin\alpha - S_2(t)\,W_2\,\mathrm{e}^{\mathrm{i}\varphi_{w_2}} = 0,\\
&-T_3(t)U_3\mathrm{e}^{\mathrm{i}\varphi_{u_3}}\sin\beta + S_3(t)\,W_3\mathrm{e}^{\mathrm{i}\varphi_{w_3}}\cos\beta - T_2(t)U_2\,\mathrm{e}^{\mathrm{i}\varphi_{u_2}} = 0,\\
&T_3(t)\,U_3\mathrm{e}^{\mathrm{i}\varphi_{u_3}}\cos\beta + S_3(t)\,W_3\,\mathrm{e}^{\mathrm{i}\varphi_{w_3}}\sin\beta - T_2(t)U_2\mathrm{e}^{\mathrm{i}\varphi_{u_2}} = 0.
\end{aligned} \tag{25}$$

The information contained within the force balance equation (21) and this geometrical compatible equation (25) allows the traction forces $T_j(t)$ and shear forces $S_j(t)$ in each rod C to be determined.

3.2. POWER FLOW IN THE INDETERMINATE THREE-ROD SYSTEM

The real input power to each rod at connection point C is given by

$$q_j(t) = \mathrm{Re}\{\dot{u}_j(t)\}\,\mathrm{Re}\{T_j(t)\} + \mathrm{Re}\{\dot{w}_j(t)\}\,\mathrm{Re}\{S_j(t)\}, \tag{26}$$

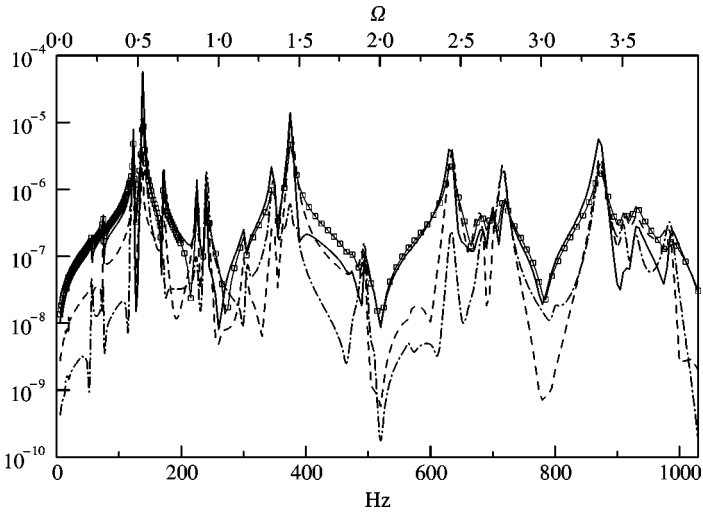

Figure 5. The variation with frequency of the amplitudes of the input power flows (W) in the three rods $q_j, j = 1, 2, 3$ and excitation q_{in}: ——, q_1; – – –, q_2; –·–·–, q_3; —□—, q_{in}.

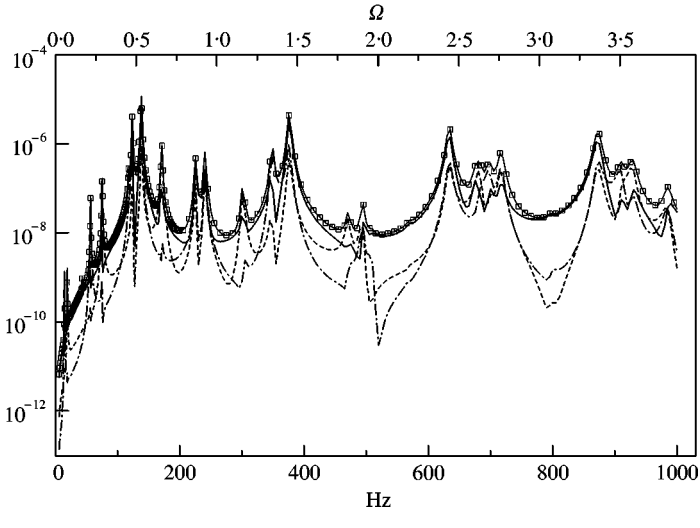

Figure 6. The variation with frequency of the amplitudes of the time-averaged input power flows (W) in the three rods $\langle q_j(t)\rangle$ and excitation $\langle q_{in}(t)\rangle$: ——, $\langle q_1\rangle$; – – –, $\langle q_2\rangle$; –·–·–, $\langle q_3\rangle$; —□—, $\langle q_{in}\rangle$.

for $j = 1, 2, 3$. The substitution of equations (20), (23) and (24) into the previous equation gives

$$\begin{aligned} q_j(t) &= \mathrm{Re}\{U_j T_j e^{i(\omega t + \varphi_{T_j} + \varphi_{u_j})}\}\mathrm{Re}\{T_j e^{i(\omega t + \varphi_{T_j})}\} + \mathrm{Re}\{W_j S_j e^{i(\omega t + \varphi_{S_j} + \varphi_{w_j})}\}\mathrm{Re}\{W_j e^{i(\omega t + \varphi_{S_j})}\} \\ &= \tfrac{1}{2} U_j T_j^2 [\cos \varphi_{u_j} + \cos(2\omega t + 2\varphi_{T_j} + \varphi_{u_j})] \\ &\quad + \tfrac{1}{2} W_j S_j^2 [\cos \varphi_{w_j} + \cos(2\omega t + 2\varphi_{S_j} + \varphi_{W_j})] \\ &= \tfrac{1}{2} (U_j T_j^2 \cos \varphi_{u_j} + W_j S_j^2 \cos \varphi_{w_j}) + A_j \cos(2\omega t + \varphi_j) \end{aligned} \tag{27}$$

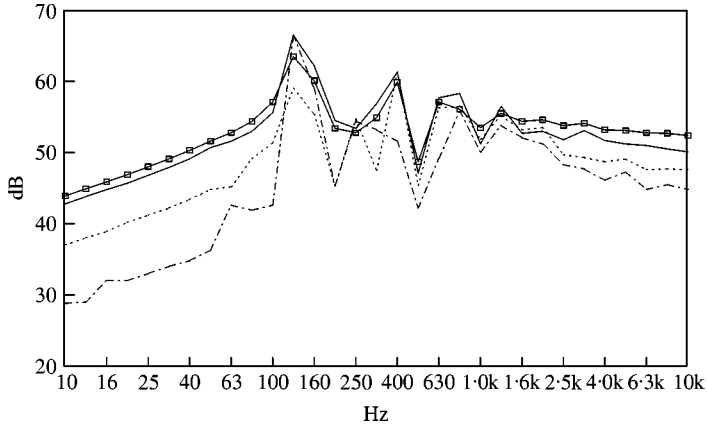

Figure 7. The corresponding information to Figure 6 expressed in a one-third octave scale (Ref. power 10^{-12} W): ——, q_1; ----, q_2; –·–·–, q_3; —□—, q_{in}.

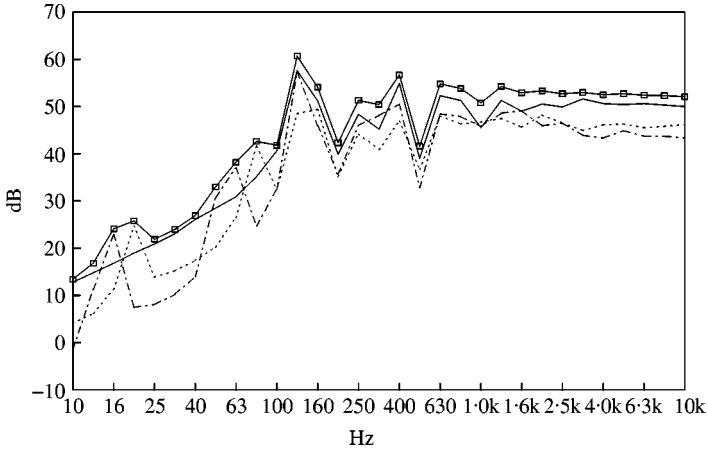

Figure 8. The corresponding information to Figure 7 expressed in a one-third octave scale: ——, $\langle q_1 \rangle$; ----, $\langle q_2 \rangle$; –·–·–, $\langle q_3 \rangle$; —□—, $\langle q_{in} \rangle$.

and its time-averaged value over a period T of excitation is

$$\langle q_j(t) \rangle = \frac{1}{T} \int_0^T q_j(t)\, \mathrm{d}t = \frac{1}{2} U_j T_j^2 \cos \varphi_{u_j} + \frac{1}{2} W_j S_j^2 \cos \varphi_{w_j}, \tag{28}$$

where

$$\varphi_j = \cos^{-1} \left[\frac{U_j T_j^2 \cos(2\varphi_{T_j} + \varphi_{u_j}) + W_j S_j^2 \cos(2\varphi_{S_j} + \varphi_{w_j})}{A_j} \right],$$

$$A_j = \tfrac{1}{2} [(U_j T_j^2 \cos(2\varphi_{T_j} + \varphi_{u_j}) + W_j S_j^2 \cos(2\varphi_{S_j} + \varphi_{w_j}))^2$$

$$+ (U_j T_j^2 \sin(2\varphi_{T_j} + \varphi_{u_j}) + W_j S_j^2 \sin(2\varphi_{S_j} + \varphi_{w_j}))^2]^{1/2}.$$

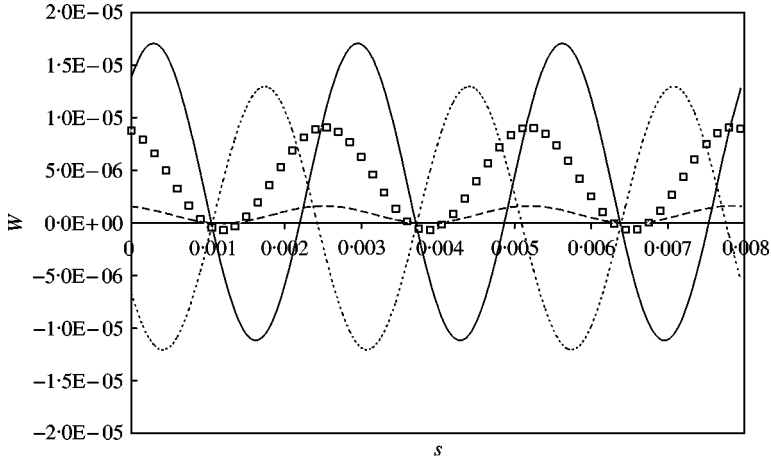

Figure 9. The variation with time of the input power flows in the three rods $q_j(t)$ and the excitation $q_{in}(t)$ at an exciting frequency of 375 Hz and angle of application of force, $\gamma = 45^\circ$ (see, Figure 4): ——, $q_1(t)$; ----, $q_2(t)$; –·–·–, $q_3(t)$; —□—, $q_{in}(t)$.

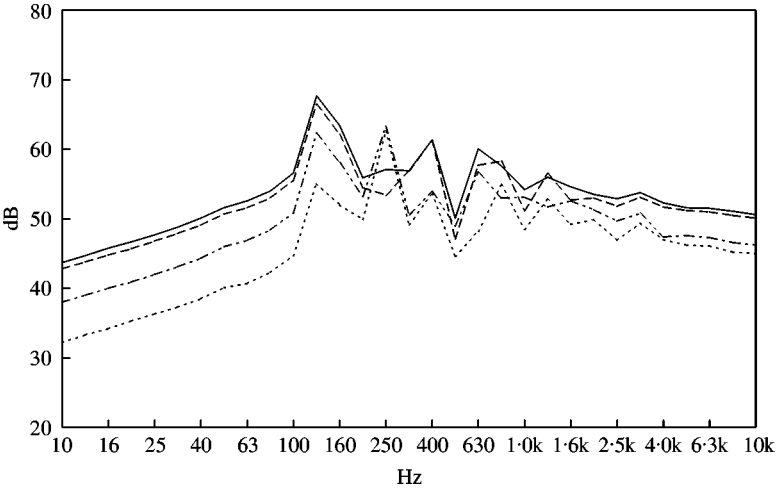

Figure 10. The variation with frequency of the amplitudes of the input power flow $q_1(t)$ to rod 1 (see, Figure 4) expressed in a one-third octave scale for different angles of application of force γ: ——, 0; – – –, 45; ----, 90; –··–, 135.

The combination of these last two equations gives

$$q_j(t) = \langle q_j(t) \rangle + \langle q_j(t) \rangle \frac{\cos(2\omega t + \varphi_j)}{\cos \varphi_j}, \tag{29}$$

indicating that the power flow in each rod contains a component equal to its time-averaged power flow value and hence is constant in time but varying with the frequency of excitation. Due to the influence of structural damping, $\cos \varphi_j > 0$, since $\varphi_j \neq 90^\circ$ and this component reduces in value as $\eta \to 0$. The dynamic component has an oscillatory behaviour of double the frequency of excitation. The instantaneous power flow $q_j(t)$ expressed in equation (27) or

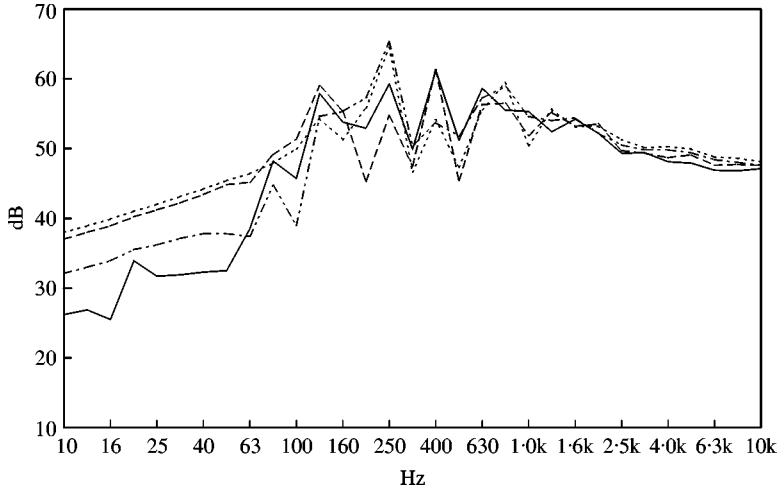

Figure 11. The variation with frequency of the amplitudes of the input power flow $q_2(t)$ to rod 2 (see, Figure 4) expressed in a one-third octave scale for different angles of application of force γ: ——, 0; – – –, 45; ----, 90; –·–·–, 135.

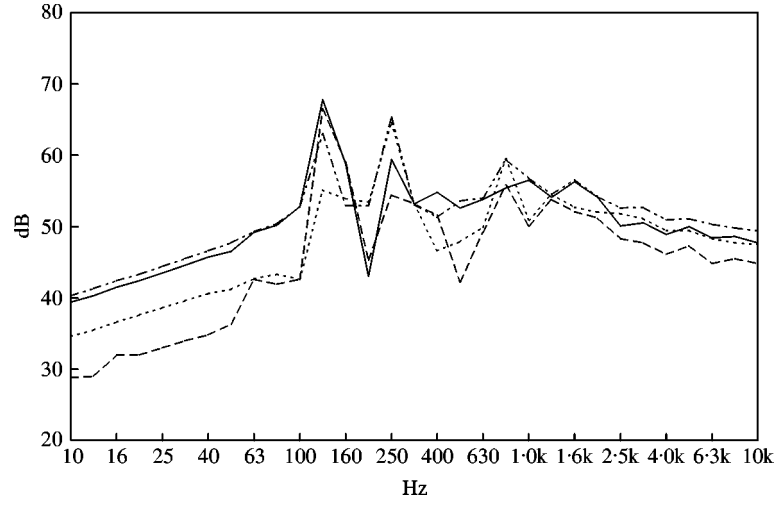

Figure 12. The variation with frequency of the amplitudes of the input power flow $q_3(t)$ to rod 3 (see, Figure 4) expressed in a one-third octave scale for different angles of application of force γ: ——, 0; – – –, 45; ----, 90; –·–·–, 135.

(29) is similar in form to equation (19) and the instantaneous sound intensity component derived by Fahy [25] and Bobrovnitskii [26]. It contains two components: an active component, with a non-zero time-averaged value, corresponding to local transport of the energy and a reactive component, with a zero time-averaged value, corresponding to local oscillatory transport of energy.

Similarly, the input power at C due to the external exciting force is given by

$$q_{in}(t) = \mathrm{Re}\{v_c(t)\}\,\mathrm{Re}\{f(t)\} \tag{30}$$

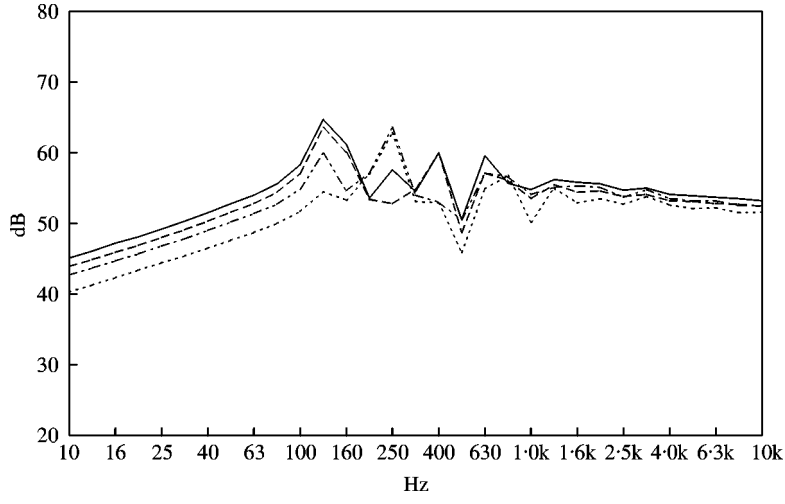

Figure 13. The variation with frequency of the amplitudes of the excitation power flow $q_{in}(t)$ expressed in a one-third octave scale for different angles of application of force γ (see, Figure 4): ——, 0; – – –, 45; ----, 90; –···–, 135.

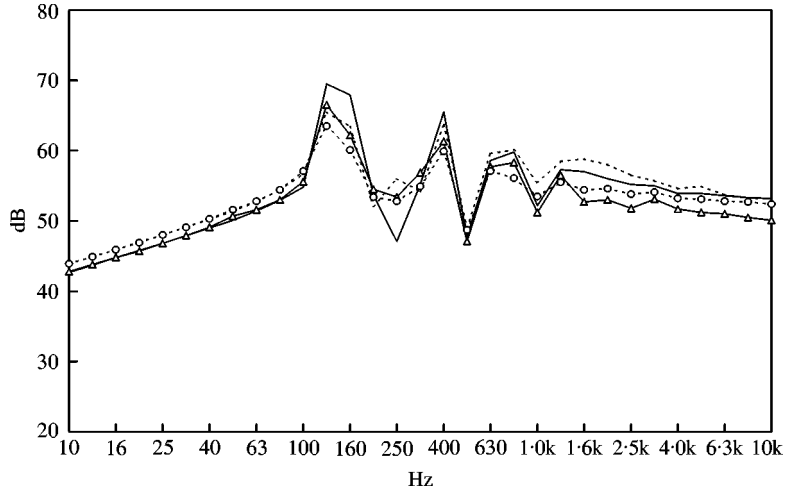

Figure 14. The variation with frequency of the amplitudes of the power flow $q_1(t)$ in rod 1 and excitation $q_{in}(t)$ expressed in a one-third octave scale: —△—, q_1 – including bending influence; --○--, q_{in} – including bending influence; ——, q_1 – not including bending influence; ----, q_{in} – not including bending influence.

with a corresponding averaged quantity $\langle q_{in}(t)\rangle$, where $v_c(t)$ is the velocity along the direction of exciting force $f(t)$ at point C. From the geometrical compatibility condition, the input power at C due to the external exciting force becomes

$$q_{in}(t) = \mathrm{Re}\{\dot{u}_2(t)\}\,\mathrm{Re}\{f(t)\}\sin\theta + \mathrm{Re}\{\dot{w}_2(t)\}\,\mathrm{Re}\{f(t)\}\cos\theta \tag{31}$$

with the corresponding time-averaged quantity $\langle q_{in}(t)\rangle$.

It is interesting to note that expressions for the power flow balance condition at C may be obtained by multiplying equations (21) and (25) by the velocity at C. Unfortunately,

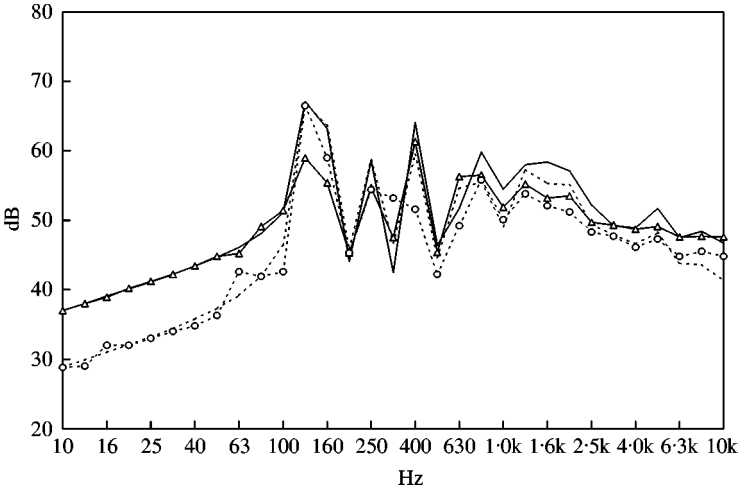

Figure 15. The variation with frequency of the amplitudes of the power flow $q_2(t), q_3(t)$ in rods 2, 3, respectively, expressed in a one-third octave scale: —△—, q_2 – including bending influence; --○--, q_3 – including bending influence; ——, q_2 – not including bending influence; ----, q_3 – not including bending influence.

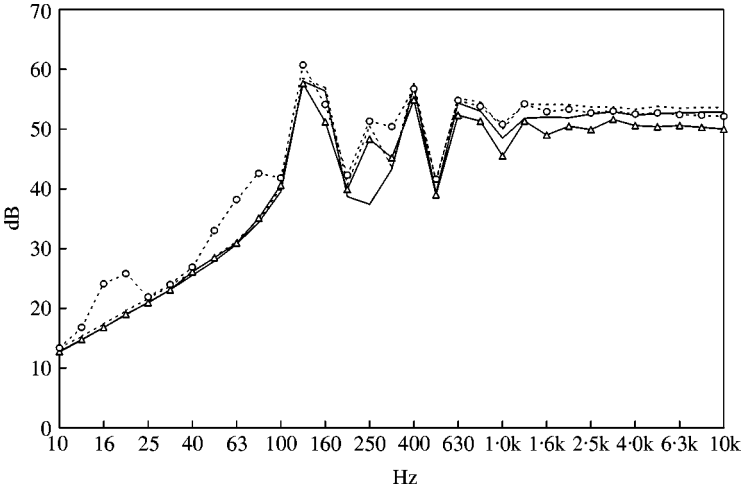

Figure 16. The variation with frequency of the amplitudes of the time-averaged power flow $\langle q_1(t)\rangle$ in rod 1 and excitation $\langle q_{in}(t)\rangle$ expressed in a one-third octave scale: —△—, $\langle q_1\rangle$ – including bending influence; --○--, $\langle q_{in}\rangle$ – including bending influence; ——, $\langle q_1\rangle$ – not including bending influence; ----, $\langle q_{in}\rangle$ – not including bending influence.

in this form, these balance equations are difficult to handle in terms of deriving solutions of power flows. The basic power flow balance equation from equation (21) at C is given by

$$q_{in}(t) = q_1(t) + q_2(t) + q_3(t) \tag{32}$$

with time-averaged quantity,

$$\langle q_{in}(t)\rangle = \langle q_1(t)\rangle + \langle q_2(t)\rangle + \langle q_3(t)\rangle. \tag{33}$$

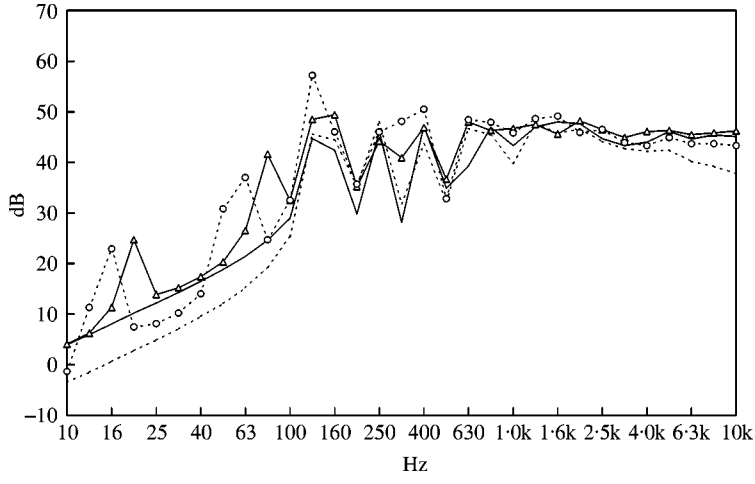

Figure 17. The variation with frequency of the amplitudes of the time-averaged power flow $\langle q_2(t)\rangle$, $\langle q_3(t)\rangle$ in rods 2, 3, respectively, expressed in a one-third octave scale: —△—, $\langle q_2\rangle$ – including bending influence; --○--, $\langle q_3\rangle$ – including bending influence; ——, $\langle q_2\rangle$ – not including bending influence; ----, $\langle q_3\rangle$ – not including bending influence.

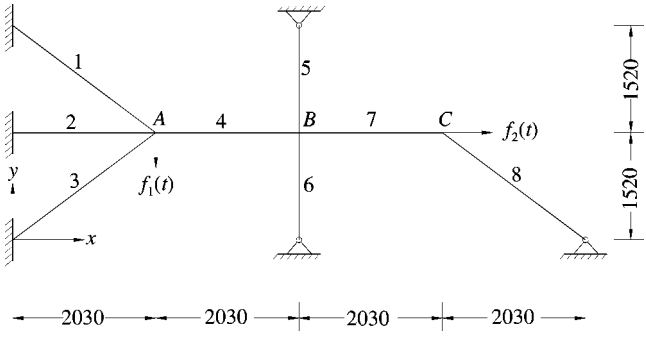

Figure 18. A beam frame with eight members of lengths measured in millimetres [18].

3.3. CALCULATION EXAMPLE 1

For illustrative purposes, it is assumed that the indeterminate system is defined by the data set:

$$l_1 = 10\text{ m}, \quad l_2 = 5\text{ m}, \quad l_3 = 5{\cdot}7735\text{ m}, \quad A_1 = 0{\cdot}04\text{ m}^2 = A_2 = A_3,$$

$$I_1 = I_2 = I_3 = 1{\cdot}333 \times 10^{-4}\text{ m}^4,$$

$$\rho = 7{\cdot}8\text{ g/cm}^3, \quad E = 2{\cdot}1 \times 10^{11}\text{ N/m}^2, \quad \eta = 0{\cdot}015, \quad \alpha = 60^\circ, \quad \beta = 30^\circ, \quad F = 1{\cdot}0\text{ N}.$$

The largest natural frequency for both compressive and bending vibration in each rod is chosen to be greater than 10 times the calculated frequency.

In the following presentation of predictions of power flow variation with frequency or time, Figures 5–9 relate to condition $\gamma = 45^\circ$ (see Figure 4). Figure 5 illustrates the variation of the amplitude of power flow with frequency ω and non-dimensional frequency

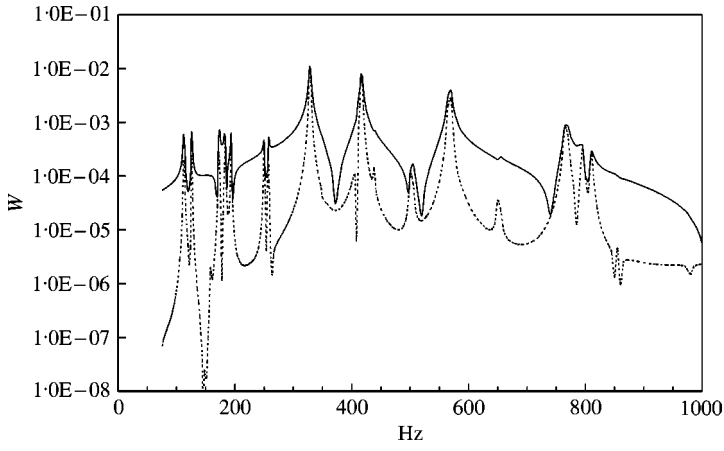

Figure 19. The variation with frequency of the amplitudes of the power flow in junction A: ——, amplitude of instantaneous power flow; ----, amplitude of time-averaged power flow.

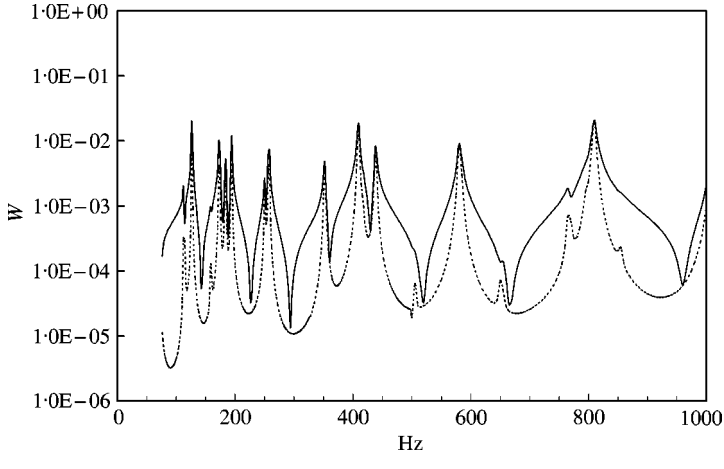

Figure 20. The variation with frequency of the amplitudes of the power flow in junction C: ——, amplitude of instantaneous power flow; ----, amplitude of time-averaged power flow.

Ω ($\Omega = \omega l_1 \sqrt{\rho/E}/\pi$) in each rod at C (i.e., equation (27)) and the excitation power flow given by equation (30). Figure 6 shows their time-averaged quantities, i.e. $\langle q_j(t) \rangle$ and $\langle q_{in}(t) \rangle$. Figures 7 and 8 present the same information in terms of one-third octave value. Figure 9 illustrates the time variation of the power flow quantities under investigation at an exciting frequency $f_n = 375$ Hz. Figures 10–13 show a selection of power flow results for $\gamma = 0, 45, 90$ and 135°, allowing comparison with Figures 5–8 to evaluate the effect of angle of application of the external excitation on the dynamic characteristics of the indeterminate system.

Although the instantaneous excitation input power $q_{in}(t)$ is equal to the sum of the three input powers of each rod, as observed in equation (32) and Figure 9, its value is not necessarily larger than the individual quantities. This is due to the influence of resonance and the manner in which energy is transferred within the overall system. For example, the

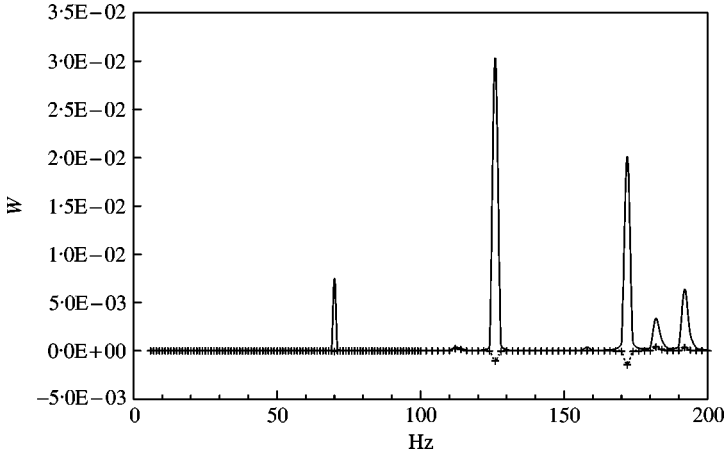

Figure 21. The variation with frequency of the time-averaged power flow in junctions *A* and *C*: -- +--, junction A; ——, junction C.

amplitude $q_1(t)$ is much larger than the amplitudes of $q_3(t)$ or $q_{in}(t)$ but at any instant their phasing is such that the energy in the total system remains in balance.

In contrast, as shown in Figures 6 and 10, the time-averaged excitation power $\langle q_{in}(t)\rangle$ is always greater in value than the other time-averaged quantities. This is due to the fact that in any period, the time-averaged power of excitation is equal to the rate of total energy dissipation of the system (see, for example, references [1, 3, 13]) and is equal to the sum of the energy dissipations in each rod (see equation (33)). As demonstrated in equation (28), each time-averaged quantity $\langle q_j(t)\rangle$ contains a constant component contribution to the overall dynamics of the system, depending on both the amplitude of the instantaneous input power and the phase angle between the velocity response and the traction and shear forces. Their peak values occur at resonance because both values of amplitude of power and $\cos \varphi_{u_j}$ or $\cos \varphi_{w_j}$ are largest.

In the low-frequency band range, Figures 7 and 8 show both the instantaneous power and time-averaged power influenced by resonance but this diminishes with increasing frequency values. For frequencies greater than 1·25 kHz, both instantaneous and time-averaged input powers expressed in the one-third octave scale range are stable in form. This is due to the presence of more modes and an increased influence of damping in the higher frequency band range, indicating that SEA is an appropriate analysis tool over 1·25 kHz.

For the indeterminate system under examination, input power depends on the excitation, dynamic and geometrical characteristics of the structures. It can be seen clearly from the selected results shown in Figures 10–13 that the input power of excitation and the power flow in each rod is related to the angle of excitation (Figure 4).

For illustrative and comparison purpose, Figures 14–17 relate to condition $\gamma = 45^\circ$ (see Figure 4) and show a set of results including and excluding bending influences. That is, in the latter case, only the compressive response of the rod is considered. Figures 14 and 15 illustrate the variation of the amplitude of power flow with one-third octave in each rod at C and the excitation power. Figures 16 and 17 show their time-averaged quantities.

Although there are many bending modes in the rod–truss system, the amplitudes of instantaneous and time-averaged power flow in each rod at C and the excitation power flow have similar levels of magnitude in the middle- and high-frequency ranges for both

conditions examined. There are obvious resonant bending mode influences below and near the first natural frequency of compressive vibration of the rod. These resonant influences in a time-averaged power flow analysis become larger and more noticeable because time-averaged power depends on both values of amplitude of power and cos φ_{u_j} or cos φ_{w_j} (see, equation (28)) with cos φ_{w_j} largest in the bending resonant condition.

3.4. CALCULATION EXAMPLE 2

The second example shown in Figure 18 is a more complex system constructed using eight beam members. Their material and geometric properties are as follows: $E = 207$ GPa, $\rho = 7860$ kg/m^3, $\eta = 0{\cdot}01$; section area of beams (1), (3), (5), (6), (7) $= 203 \times 203$ mm^2, section area of beams (2), (4), (8) $= 152 \times 152$ mm^2. The frame is loaded at junctions A and C by harmonic forces $f_1(t) = 22{\cdot}25\mathrm{e}^{\mathrm{i}\omega t}$ N and $f_2(t) = 44{\cdot}5\mathrm{e}^{\mathrm{i}\omega t}$ N respectively. This system was originally examined by Beale and Accorsi [18] in assessing its dynamic characteristics by adopting a travelling wave model.

Similar to the calculations described in Example 1, a modal substructure approach is again used to calculate the power flow utilizing the force (moment) balance equations and geometrical compatibility equations at junctions A–C. The substructure boundary conditions used here are one end fixed, one end free for beams (1)–(3), two free ends for beams (4), (7) and one end simply supported, one end free for beams (5), (6), (8). The expressions describing power flow at a junction are similar to those given in equations (31)–(33). The power flow at a junction is zero (for example, junction B) if there is no applied external excitation force at this position because of the balance between internal forces and continuous displacements.

Figures 19–21 illustrate the variation of the amplitude of power flow with frequency at junctions A and C. The calculated time-averaged power flow values at junctions A and C demonstrate the same trends as those presented by Beale and Accorsi [18]. From Figure 21, it is observed that the time-averaged power flow at junction A produces negative values at several exciting frequencies implying that the direction of the exciting force $f_1(t)$ and the velocity are opposite to one another. This means that the exciting force source $f_1(t)$ at junction A absorbs power from the system and it behaves as an active control source at these frequencies.

4. CONCLUSIONS

Based on a dynamic substructure approach, the power flow of an indeterminate rod system is calculated by combining the force balance equations with geometrical compatibility equations. The power flow in each rod is strongly related to its dynamic response and it may be larger than the input power of excitation due to resonance. When only one excitation source exists, it was shown that the time-averaged input power of excitation is always greater in value than the other time-averaged quantities. But when several excitation sources are applied at the same time, the time-averaged input power of an exciting source may be negative and is behaving as an active control source. The input power depends on the excitation, geometrical and dynamical characteristics of the subsystems. The instantaneous power flow in each rod is represented by a constant component in time equal to its time-averaged power flow value and a dynamic component of double the frequency of excitation and an amplitude related to the time-averaged power flow, i.e., $\langle q_j(t)\rangle/\cos\varphi_j$, see equation (29). The resonance influences in both instantaneous

power and time-averaged quantity decrease as the frequency increases, with stable dynamic characteristics exhibited at higher frequencies (higher modal density).

REFERENCES

1. F. J. FAHY 1994 *Philosophical of Transactions of Royal Society, London* A **346**, 431–447. Statistical energy analysis: a critical overview.
2. R. H. LYON and G. MAIDANIK 1962 *Journal of the Acoustics Society of America* **34**, 623–639. Power flow between linearly coupled oscillators.
3. R. H. LYON 1975 *Statistical Energy Analysis of Dynamic Systems, Theory and Applications*. Cambridge, Massachusetts: MIT Press.
4. R. S. LANGLEY 1992 *Journal of Sound and Vibration* **159**, 483–502. A wave intensity technique for the analysis of high frequency vibration.
5. J. E. MANNING 1994 *Philosophical of Transactions of Royal Society, London* A **346**, 477–488. Formulation of SEA parameters using mobility functions.
6. A. J. KEANE and W. G. PRICE (editors) 1997 *Statistical Energy Analysis, an Overview, with Application in Structure Dynamics*. Cambridge: Cambridge University Press.
7. F. J. FAHY and W. G. PRICE (editors) 1999 *IUTAM Symposium on Statistical Energy Analysis*. Dordrecht: Kluwer Academic Publishers.
8. H. G. D. GOYDER and R. G. WHITE 1980 *Journal of Sound and Vibration* **68**, 59–75. Vibrational power flow from machines into build-up structures. I. Introduction and approximate analysis of beam and plate-like foundations.
9. H. G. D. GOYDER and R. G. WHITE 1980 *Journal of Sound and Vibration* **68**, 77–95. Vibrational power flow from machines into build-up structures. II. Wave propagation and power flow in beam-stiffened plates.
10. H. G. D. GOYDER and R. G. WHITE 1980 *Journal of Sound and Vibration* **68**, 97–117. Vibrational power flow from machines into build-up structures. III. Power flow through isolation system.
11. R. J. PINNINGTON and R. G. WHITE 1981 *Journal of Sound and Vibration* **75**, 179–197. Power flow through machine isolator to resonant and non-resonant beam.
12. J. T. XING and W. G. PRICE 1999 in *IUTAM Symposium on Statistical Energy Analysis* (F. J. Fahy and W. G. Price, editors), 83–94. Dordrecht: Kluwer Academic Publishers. The energy flow equation of continuum dynamics.
13. J. T. XING and W. G. PRICE 1999 *Proceeding of the Royal Society A* **455**, 401–436. A power-flow analysis based on continuum dynamics.
14. J. M. CUSCHIERI 1990 *Journal of the Acoustics Society of America* **87**, 1159–1165. Structural power-flow analysis using a mobility approach of a L-shape plate.
15. R. S. LANGLEY 1989 *Journal of Sound and Vibration* **135**, 319–331. Application of the dynamic stiffness method to the free and force vibrations of aircraft panels.
16. D. W. MILLER and A. VON FLOTOW 1989 *Journal of Sound and Vibration* **128**, 145–162. A travelling wave approach to power flow in structure networks.
17. J. L. HORNER and R. G. WHITE 1991 *Journal of Sound and Vibration* **147**, 87–103. Prediction of vibration power transmission through bends and joints in beam-like structures.
18. L. S. BEALE and M. L. ACCORSI 1995 *Journal of Sound and Vibration* **185**, 685–702. Power flow in two and three dimensional frame structures.
19. K. SHANKAR and A. J. KEANE 1995 *Journal of Sound and Vibration* **185**, 867–890. Energy flow predictions in a structure of rigidly joined beams using receptance theory.
20. K. SHANKAR and A. J. KEANE 1997 *Journal of Sound and Vibration* **201**, 491–513. Vibrational energy flow analysis using a substructure approach: the application of receptance theory to FEA and SEA.
21. L. MEIROVITCH 1967 *Analytical Methods in Vibration*. New York: Macmillan.
22. LORD RAYLEIGH 1894 *Theory of Sound*. London: Macmillan.
23. G. B. WARBURTON 1954 *Proceedings of the Institution of Mechanical Engineer* **168**, 371–382. The vibration of rectangular plates.
24. L. CREMER, M. HECKL and E. E. UNGAR 1988 *Structure-borne Sound*. Berlin: Springer-Verlag.
25. F. J. FAHY 1989 *Sound Intensity*. London: Elsevier Science Publishers.
26. Y. I. BOBROVNITSKII 1999 in *IUTAM Symposium on Statistical Energy Analysis* (F. J. Fahy and W. G. Price, editors), 37–46. Dordrecht: Kluwer Academic Publishers. Some energy relations for mechanical systems.